Available online at www.sciencedirect.com

ScienceDirect

journal homepage: www.elsevier.com/locate/he

Optimization of boron dispersion on fibrous-silica-nickel catalyst for enhanced CO_2 hydrogenation to methane

N.S. Hassan [a], A.A. Jalil [a,b,*], N.A.A. Fatah [b], I. Hussain [b], A.F.A. Rahman [a], S.A.M. Dolit [a], K. Kidam [a], R. Jusoh [c], M.A.A. Aziz [a], H.D. Setiabudi [c], C.K. Cheng [d]

[a] School of Chemical and Energy Engineering, Faculty of Engineering, Universiti Teknologi Malaysia, 81310 UTM Johor Bahru, JohC, Malaysia

[b] Centre of Hydrogen Energy, Institute of Future Energy, Universiti Teknologi Malaysia, 81310 UTM Johor Bahru, Johor, Malaysia

[c] Faculty of Chemical and Process Engineering Technology, College of Engineering Technology, Universiti Malaysia Pahang, Lebuhraya Tun Razak, 26300, Gambang, Kuantan, Pahang, Malaysia

[d] Center for Catalysis and Separation (CeCaS), Department of Chemical Engineering, College of Engineering, Khalifa University of Science and Technology, 127788, Abu Dhabi, United Arab Emirates

HIGHLIGHTS

- Apt boron dispersion surround nickel particles improved CO_2 adsorption.
- Boron accelerated the methanation and restricted the coke formation.
- Addition of boron onto FSN improved the nickel activity and stability.
- Optimization of methanation by FCCCD and RSM gave the highest 84.3% of methane.

GRAPHICAL ABSTRACT

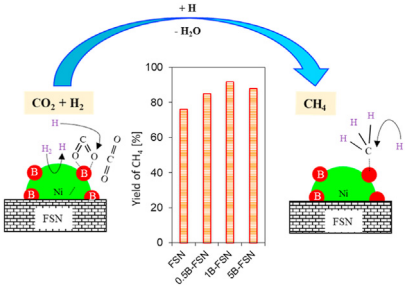

ARTICLE INFO

Article history:
Received 14 August 2021
Received in revised form
1 January 2022
Accepted 14 February 2022
Available online 5 March 2022

ABSTRACT

There are numerous reports regarding boron-containing catalysts for hydrogen-related reactions from CO_2 including dry reforming of methane and methanation. Besides enhancing the productivity, boron also improved nickel activity and stability. However, the detailed mechanistic study, particularly in explaining the starring role of boron in the enhanced reactions, is still lacking. Thus, herein we loaded boron on fibrous-silica-nickel and investigated their physicochemical properties and mechanistic route by means of in-situ FTIR for enhanced CO_2 methanation. It was found that the appropriate dispersion of

* *Coresponding author*. School of Chemical and Energy Engineering, Faculty of Engineering, Universiti Teknologi Malaysia, 81310, UTM Johor Bahru, Johor, Malaysia.
E-mail address: aishahaj@utm.my (A.A. Jalil).

https://doi.org/10.1016/j.ijhydene.2022.02.126

Keywords:
Nickel
Boron
Basic sites
CO_2 hydrogenation
Methane
Optimization

boron surrounds the nickel particles is an important factor to improve the adsorption of CO_2 before interacting with split hydrogen atom from the nickel sides to form intermediates which are subsequently dehydrated, and then serial hydrogenation gave the final product of methane. Boron also accelerated the methanation and restricted coke formation. A hybrid approach on optimization via a face-centered central composite design and a response surface methodology showed that reaction using H_2/CO_2 ratio of 6, GHSV of 10,500 mL g^{-1} h^{-1}, at 500 °C gave the highest percentage of CH_4 of 84.3%. To indicate the error, the predicted values were compared to the experimental values, yielding an accurately minimal error ranging from 0 to 11%. As a result, the empirical models generated for CO_2 hydrogenation to methane were reasonably accurate, with all actual values for the confirmation runs fitting within the 94% prediction interval.

Introduction

Continuous depletion of conventional energy sources and global warming are the two main factors that putting our environment sustainability at risk [1]. Thus, this phenomenon has led to the search for renewable energy sources, which can be achieved by converting carbon dioxide (CO2) greenhouse gas into a useful energy carrier. CO_2 hydrogenation into methane (CH_4) provides an effective solution towards the CO_2 mitigation, and the CH_4 is useful as fuel [2]. The catalytic CO_2 methanation to produce synthetic natural gas is a highly exothermic reaction that is frequently catalyzed by metal-supported catalysts [3]. In this case, developing an efficient catalyst that can operate at low temperatures and is applicable as highly thermal conduction material is particularly preferred.

Ni-based catalysts are well explored among the researched catalysts because of their high catalytic activity and low cost compared to noble metals (Ru, Rh, and Pd) [4–6]. However, several problems have been addressed on applying those catalysts, such as coking, sintering, and chemical poisoning [7]. In order to overcome this problem, many studies have focused on the catalyst synthesis procedure to control the Ni particle size, its dispersion on support materials, and the metal-support interaction, which acts as key factors in the catalytic CO_2 methanation [8]. Liu et al. recently described a simple one-pot synthesis of NiO loaded on SBA-15 that has anti-sintering capabilities and greater catalytic activity than the same catalyst synthesized by the impregnation approach [9]. Similarly, the mechanochemical method such as solid-state reaction was used for the synthesis of Co–Ni/Al_2O_3, and the catalyst had the highest catalytic performance in CO_2 methanation (76.2% CO_2 conversion and 96.39% CH_4 selectivity at 400 °C) as well as high stability over 10 h time-onstream [10]. Other than that, the alteration of SBA-15 into fibrous SBA-15 boosted the accessibility of the bulk active sites onto support, resulting in outstanding catalytic efficiency and stability of the catalyst [11]. Indeed, the preparation procedure has resulted in a crucial effect on the morphology and manipulating the catalyst's activity and stability [12,13].

The addition of promoter onto nickel-based catalysts is also a remarkable way for improving the Ni activity and stability. Recently, boron has gained significant research interests as a promoter due to its excellent tendency to mitigate coke nucleation sites. For instance, boron has been reported as a good promoter for methane steam reforming [14], Fischer–Tropsch catalysts [15,16], propane dehydrogenation over Pt/γ-Al_2O_3 [17], and hydrogen storage [18]. In past decades, the effect of boron on Al_2O_3-supported nickel catalysts has been investigated for dry reforming of methane. For example, low amounts of boron (0.6–5.6 wt% B_2O_3) considerably improve the dispersion of the nickel-supported phase and reduce the carbon deposition [19]. In another study, it was noticed that a lower concentration of boron (1 and 2%) was more favorable to achieve the higher catalytic activity, whereas the higher concentration (3% and 5%) resulted in a comparatively lower conversion for CH_4 and CO_2 [20]. Interestingly, an unpromoted catalyst showed 14% carbon deposition and was reduced to 1.3% for 2% boron-promoted catalyst due to B–OH species' presence on the catalyst surface. Thus, boron is revealed could preclude the surface of catalysts from deposition and growth of carbon species that were responsible for coking.

Recently, we have successfully synthesized a highly active and stable nickel loaded on fibrous silica KCC-1 (KAUST Catalysis Centre 1) catalyst by in-situ one-pot hydrothermal method, which converted CH_4 (92%) and CO_2 (88%) to high H_2/CO ratio, and had exceptional stability over 72 h TOS at 750 °C [21]. Further modification of the Ni@KCC-1 with La_2O_3 was found to enhance the selectivity of H_2/CO products to values close to unity. However, the stability slightly dropped if compared with the pristine Ni@KCC-1. Therefore, as an extension of this study and inspired by significant findings of boron, herein we attempted to incorporate boron onto Ni@KCC-1 (denoted as fibrous-silica-nickel (FSN) catalyst) in order to explore the behaviour of boron during CO_2 methanation, which is thought to improve the catalyst's activity and stability. To the best of our knowledge, no previous study has explored the combined effects of boron and FSN catalyst for CO_2 methanation. The catalyst's physicochemical properties were characterized in detail, the reaction mechanism also was

elucidated by means of FTIR as well as the optimization of CO_2 methanation was also done by a hybrid approach via a face-centered central composite design (FCCCD) and a response surface methodology (RSM).

Experimental

Synthesis procedure

Fibrous silica nickel was obtained via a one-pot synthesis procedure by adding 4.54 g of Ni metal precursor ($Ni(NO_3)_2 \cdot 6H_2O$) into the colloidal mixture of fibrous silica, which the colloidal solution was prepared according to the steps in literature [22]. The metal-loaded mixture was mixed until homogeneous before it was transferred into an autoclave for the aging process (3 h, 120 °C). After that, the solution was centrifuged to remove the solution before it was dried overnight in an oven. Then, the catalyst in powder form was calcined (6 h, 550 °C), and the final product was denoted as FSN.

Boron-loaded FSN was prepared using boric acid as a precursor via the wet impregnation method. Briefly, 0.0287 g of boric acid was added into a solution containing 1 g of FSN in distilled water under stirring at 40 °C. The resulting solution was stirred (30 min, 50 °C). After that, the temperature rose to 80 °C, and the solution was continuously stirred until it became a thick paste. Then, the sample was dried in an oven (12 h, 110 °C) andcalcined (3 h, 550 °C). The final product was denoted as xB/FSN (x = 0.5, 1 and 5 wt% of boron).

Catalyst characterization

The catalyst's crystallinity was obtained by an X-Ray diffractometer (Bruker Advance D8 X-ray) using 40 mA and 40 kV from Cu kα radiation source. The catalyst's textural characteristics were analyzed from nitrogen physisorption recorded on Beckman Coulter analyzer (SA3100). The BET method and nonlocal density functional theory (NLDFT) were utilized to calculate specific surface areas, pore volumes, and pore size distributions (PSD) using adsorption data. FESEM (IEOL ISM-6701F) was used to analyze the morphological properties of the catalysts. A Bruker Advance 400 MHz 9.4T spectrometer was used to capture ^{11}B NMR spectra.

Catalytic performance test for CO_2 methanation

At reaction temperatures of 150–500 °C, a fixed bed reactor was used for catalytic testing with equipped with a thermocouple. The catalyst in the form of a 20–40 μm fraction (0.2 g) was created by the sieving process and fed into the reactor. Prior to the catalytic reaction, the catalyst was pretreated for 1 h and then reduced under hydrogen for 4 h at 400 °C under air flow (F_{Oxygen} = 100 mL. min^{-1}) and ($F_{Hydrogen}$ = 100 mL. min^{-1}), respectively. The CO_2 and H_2 have then flowed in a 1:4 stoichiometric ratio before passing through the catalyst and being transferred to the gas chromatography system (GC, 6090 N Agilent GC). Using a TCD detector and a GSCarbon PLOT type column, the component of the output gases was measured. The following equation was used to calculate selectivity, CH_4 yield, and CH_4 production rate:

$$\text{Selectivity of } CH_4 = \frac{[\text{mole } CH_4]_{out}}{[\text{mole } CH_4]_{out} + [\text{mole CO}]_{out}} \quad (1)$$

$$CH_4 \text{ Yield } (\%) = \frac{[\text{mole } CH_4]_{out}}{[\text{mole } CH_4]_{out} + [\text{mole CO}]_{out}} \times \frac{[\text{mole } CO_2]_{in} - [\text{mole } CO_2]_{out}}{[\text{mole } CO_2]_{in}} \quad (2)$$

$$\text{Rate of } CH_4 \text{ formation} = \frac{[\text{mole}]_{CH_4 \text{ produced}}}{[\text{mole}]_{metal(total)} \times \text{time}} \quad (3)$$

Experimental design and optimization

CO_2 methanation was optimized over 0.5B-FSN via the statistical software package Design Expert (Version 7.1.6, State-Ease, Minneapolis, USA). The investigated parameter was chosen from three independent variables: (A) reaction temperature, (B) gas hourly space velocity, GHSV and (C) carbon dioxide to hydrogen ratio, CO_2/H_2. Using FCCCD, the influence of each variable, the sum of squares, mean square, *p*-value, *F*–value, and confidence level (%), on the prediction of the optimum reaction parameter were determined. The treatment time in this study is defined as the duration of the reduction treatment performed prior to the reaction. Table S1 lists the coded level and range of the response parameters evaluated, with the ranges were chosen based on the results obtained in the prior study [23]. The total number of tests completed, according to the design, is 26 with 23 factorial points, 1 axial point, and 4 replicates at the centre points, as shown in Table S2.

Results and discussion

Catalytic activity

The effect of boron loading onto fibrous-silica-nickel (FSN) toward CO_2 methanation at a temperature range of 150–525 °C was examined, and the findings are displayed in Fig. 1A. It was observed that the addition of boron up to 1 wt% onto FSN obviously increased the yield of CH_4 but further increased the boron amount to 5 wt% somehow decreased the performance as summarized in Fig. 1B, where the maximum yield of CH_4 at 525 °C was in the following order: IB-FSN (92%) > 5B-FSN (88%) > 0.5B-FSN (85%) > FSN (76%). It also clearly observed that the overall rate of methanation decelerated by the addition of boron in spite of an enhancement in the final yield of CH_4. This may be due to multistep reactions had taken place towards the CH_4 formation while preserving the stability of the catalyst. Attributable to the similar performance of CO_2 methanation over various boron-loaded FSN catalysts, hereafter, the 0.5B-FSN, which exhibited a higher reaction rate, was chosen as a model boron loaded catalyst compared with the pristine FSN. The catalyst's physicochemical characteristics were studied in detail to unravel the important role of boron on FSN in enhancing the methanation (see Fig. 2) (see Fig. 2).

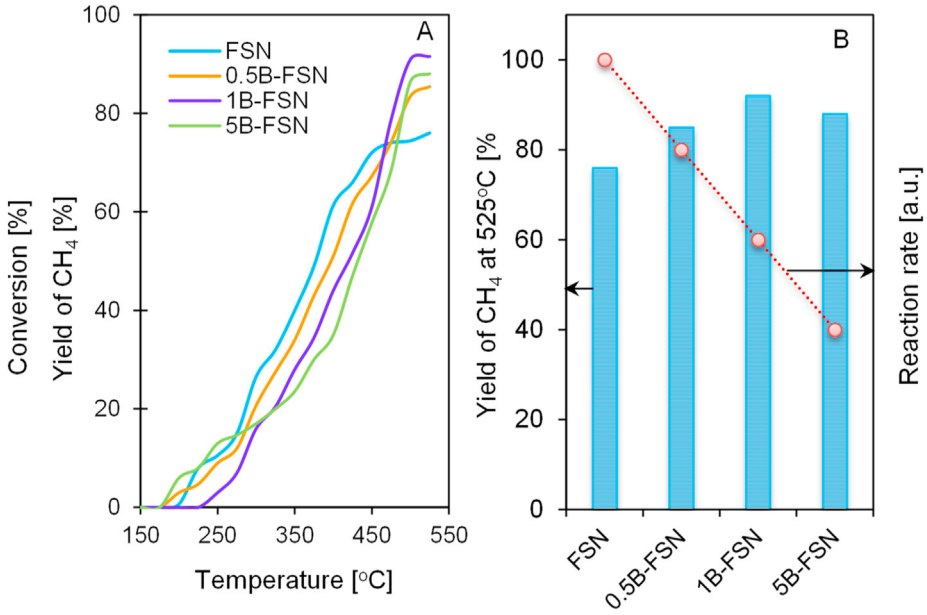

Fig. 1 – (A) CO_2 conversion and yield of CH_4 over FSN based catalysts (B) Maximum yield of CH_4 at 525 °C and overview reaction rate over FSN based catalysts.

Characterization of the catalyst

Fig. 2A illustrates that the FSN showed several diffraction peaks located at 2θ = 37.2, 43.3°, 62.8°, 75.3°, and 79.1°, which corresponded to nickel oxide (NiO) phase crystallites form (JCPDS 78–0429) [22,24]. The absence of a typical peak for boron oxide suggests that tiny boron oxide particles were widely spread on the catalyst surface, with crystallite sizes much below the XRD detection limit. According to the literature, boron oxide is seemingly difficult to crystallize and forming amorphous glassy phases [14,19]. It is seen that the diffractogram pattern of FSN and 0.5BFSN are alike with slightly higher in intensity and additional peaks for NiO appeared when boron was loaded onto the FSN. This is most probably due to the boric acid added rinsed the surface of FSN and somewhat altered the original structure of FSN to arise the nickel species.

The nitrogen physisorption experiment was performed to examine the Brunauer-Emmett-Teller (BET) surface areas and pore size distribution of both catalysts, and the findings are displayed in Fig. 2B. The catalysts had a type IV isotherm with H3 hysteresis loops, which is a common mesoporous feature [25,26]. Fig. 2C shows the NLDFT pore size distributions, and detailed analyses tabulated in Table 1 validated these findings, indicating that the increase in surface area for 0.5B-FSN compared to pristine FSN was undeniably due to the formation of the larger pore by the boron species. The smaller pores look like they were blocked, as evidenced by the decrease in micropore volume.

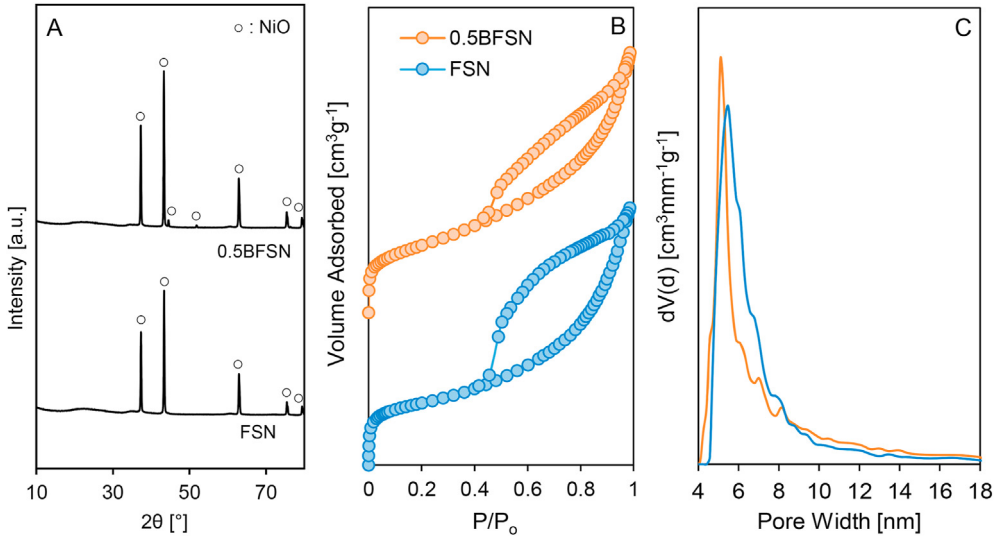

Fig. 2 – (A) XRD diffractogram of FSN based catalysts (B) Nitrogen physisorption and (C) pore size distribution of FSN based catalysts.

Table 1 – Textural properties of all catalysts.

Catalysts	Surface Area (m^2g^{-1})	Micropore Volume (cm^3g^{-1})	Mesopore Volume (cm^3g^{-1})	Total Pore Volume (cm^3g^{-1})
FSN	215	0.0319	0.3531	0.3650
0.5B-FSN	237	0.0111	0.3749	0.3640

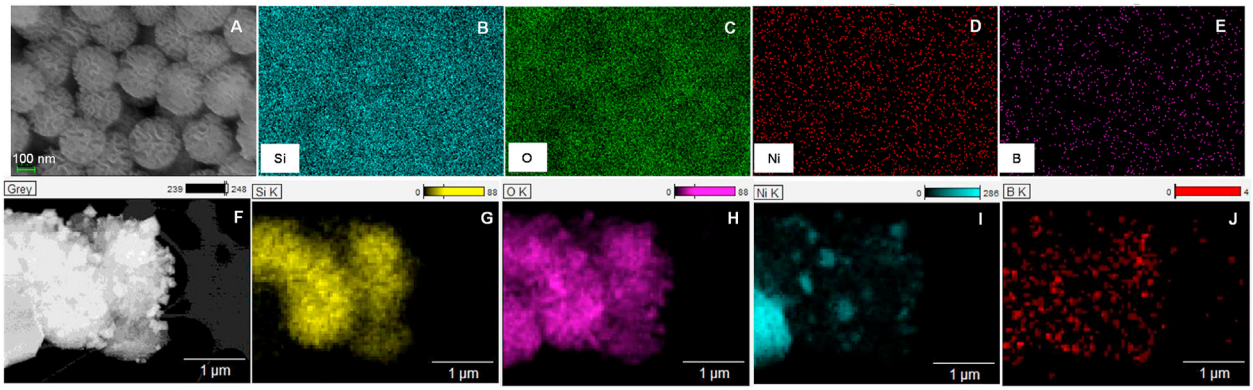

Fig. 3 – Elemental mapping of 0.5B-FSN via FESEM (A–E) and TEM (F–J).

Next, the FESEM (Fig. 3A–E) and TEM (Fig. 3F–J) images as well as elemental mapping of 0.5B-FSN, were inspected in order to elucidate the surface morphology, particle size and distribution of each species. Fig. 3A shows that the catalyst was made up of uniform microspheres of silica with a bicontinuous concentric lamellar with particles size range of 200–300 nm [22]. This image also confirmed that the fibrous structure of FSN remained intact even after the addition of boron. Fig. 3B and C portrayed the fibrous silica (Si–O–Si) framework, while the well dispersion of nickel and boron on it are clearly shown in Fig. 3D and E, respectively with the latter slightly less distributed compared to the former. The TEM-EDX mapping of the same catalyst presented in Fig. 3F–3J further proved all these results.

In order to study the detailed influence of the addition of boron onto the FSN structure, the catalysts were then subjected to FTIR and NMR analyses. The reduced intensity of FTIR spectrum of 0.5B-FSN shown in Fig. 4A clearly demonstrated that boron somehow affected the structure of FSN particularly the silica framework backbone of asymmetric Si–O–Si vibration at band 1080 cm^{-1} and the symmetric stretching of Si–O–Si at band 466 cm^{-1} at the fingerprint region [27–29]. Fig. 4B and C showed the ^{29}Si NMR spectrum for FSN and 0.5B-FSN, respectively with their deconvoluted peaks by the Gaussian curve-fitting. It can be observed that all the Q_1-Q_4 peaks for different silica coordination at −83, −91, −102 and −111 ppm, respectively reduced in intensity and slightly shifted to lower chemical shift number primarily for the Q_1 and Q_2 coordination when the boron was loaded onto FSN, indicating the interference happened in the structure of silica framework due to the possible isomorphous substitution of boron with the oxygen atom [30,31]. Similar phenomenon was also detected from the reduced band at 794 cm^{-1} in the FTIR spectrum of 0.5B-FSN shown in Fig. 4A, demonstrating the possible substitution of boron with the hydrogen atom of Si–O–H groups. Besides, the boron also most probably substituted with the nickel atom that already substituted in the silica framework during the synthesis of FSN [24]. This

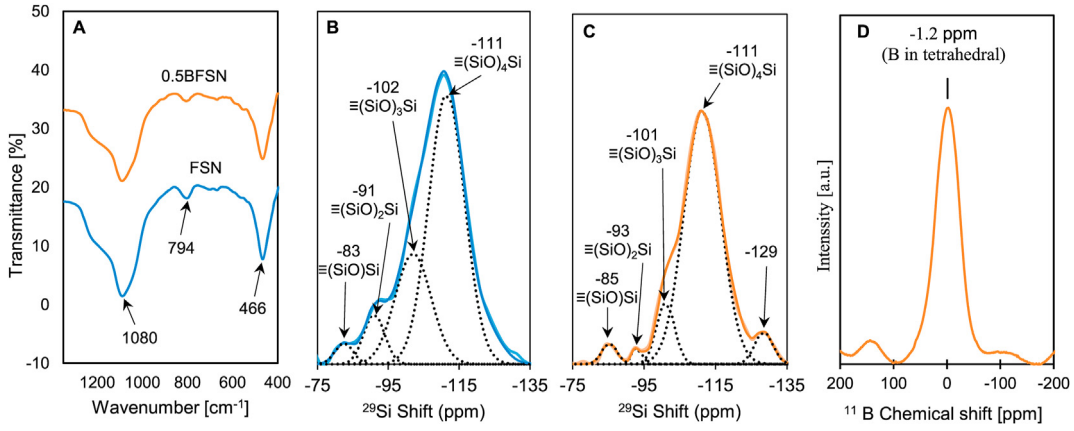

Fig. 4 – (A) FTIR spectra of FSN based catalysts, ^{29}Si NMR spectrum of (B) FSN (C) 0.5B-FSNand (D) ^{11}B NMR spectrum of 0.5B-FSN.

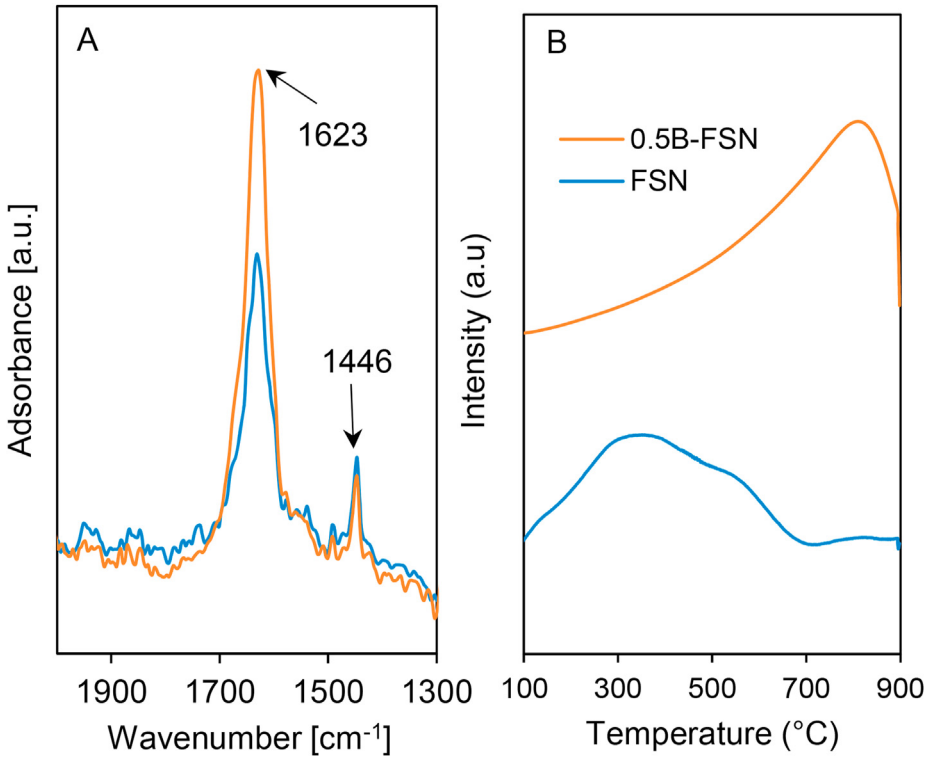

Fig. 5 – FTIR spectra of pyrrole adsorbed at room temperature (A) and CO_2–TPD observation(B) over FSN based catalysts.

may explain why the XRD diffractogram for NiO is slightly higher and more pronounced for the 0.5B-FSN compared to the pristine FSN. The presence of boron species in silica framework tetrahedral sites of 0.5B-FSN catalyst was confirmed by the single signal at −1.2 ppm in ^{11}B NMR spectrum as shown in Fig. 4D [32].

The effect of boron on the basicity of FSN was investigated by FTIR analysis with pyrrole as a probe molecule (Fig. 5A) and also by CO_2-TPD (Fig. 5B). Two main bands are obviously detected at 1623 and 1446 cm^{-1} in Fig. 5A, which corresponded to an aromatic C=C stretching vibration of the pyrrole ring and pyrolate species from the dissociation of pyrrole, respectively [33,34]. The former band for 0.5B-FSN is noticeably higher than the pristine FSN and seems vice-versa for the latter, indicated that more pyrrole was adsorbed onto the surface of 0.5B-FSN catalyst while easier to detach from the

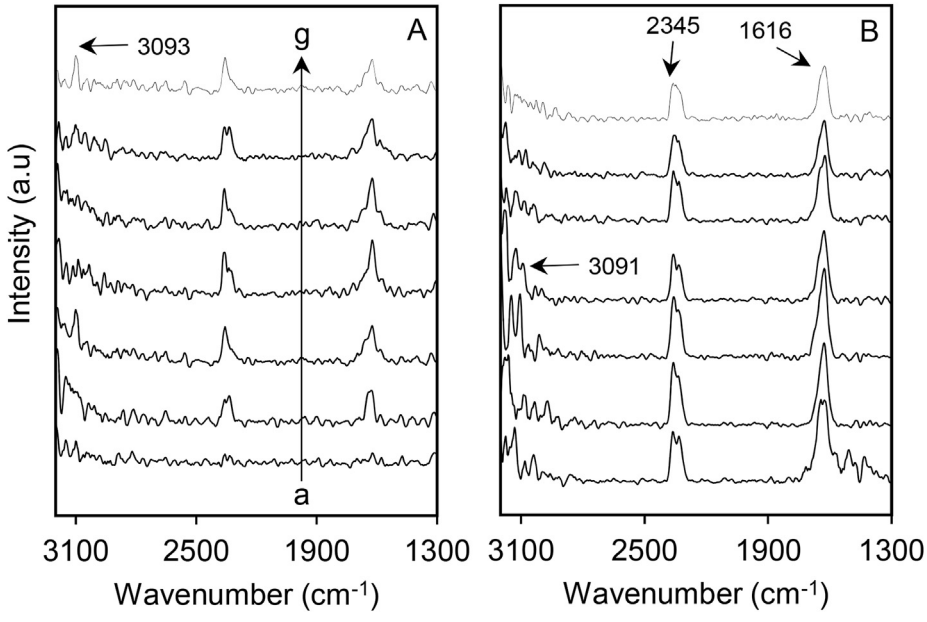

Fig. 6 – $CO_2 + H_2$ adsorbed FTIR spectra of (A) FSN (B) 0.5BFSN at (a) 100 °C(b) 150 °C (c) 200 °C (d) 250 °C (e) 300 °C (f) 350 °C (g) 400 °C.

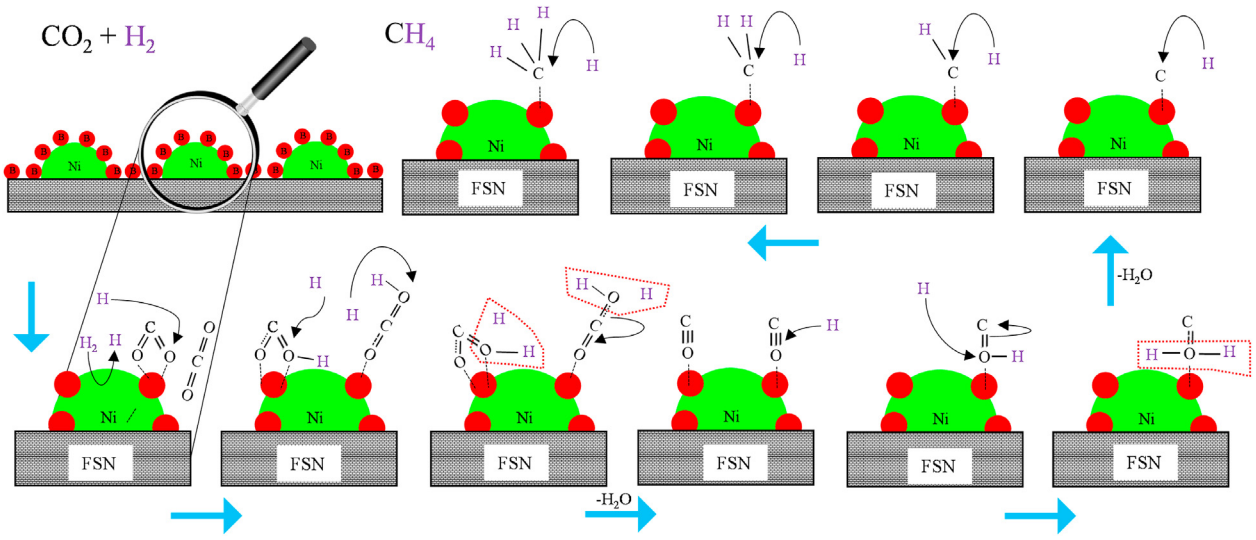

Fig. 7 – Proposed reaction mechanism for CO_2 methanation over 0.5B-FSN.

FSN surface, meaning such an amount of basicity has been increased by the addition of merely 0.5 wt% boron onto the FSN. This improvement would be one of the reasons for the higher performance of 0.5B-FSN compared to the pristine FSN shown in Fig. 1. The strength of basicity also extremely increased by the addition of boron onto FSN as shown by the CO_2-TPD result in Fig. 5B, whereby the maximum CO_2 desorbed shifted from 343 °C for the pristine FSN to 820 °C for the 0.5B-FSN. It is expected that this enhanced property also would be beneficial for the stability of the catalyst toward CO_2 methanation.

Proposed mechanism of CO_2 methanation over 0.5B-FSN

In order to correlate all the above-mentioned catalytic activity and characterization results with the role of boron toward CO_2 methanation, both pristine FSN and 0.5B-FSN catalysts were analyzed by *in-situ* $CO_2 + H_2$ adsorbed FTIR at elevated temperature of 100 °C – 400 °C, and the results are shown in Fig. 6. Generally, two main bands are detected at 2345 and 1616 cm^{-1} in both figures, which are ascribed to linear gaseous CO_2 and atomic hydrogen, respectively [27,33,35]. The bands intensity for pristine FSN (Fig. 6A) is somehow less pronounced as

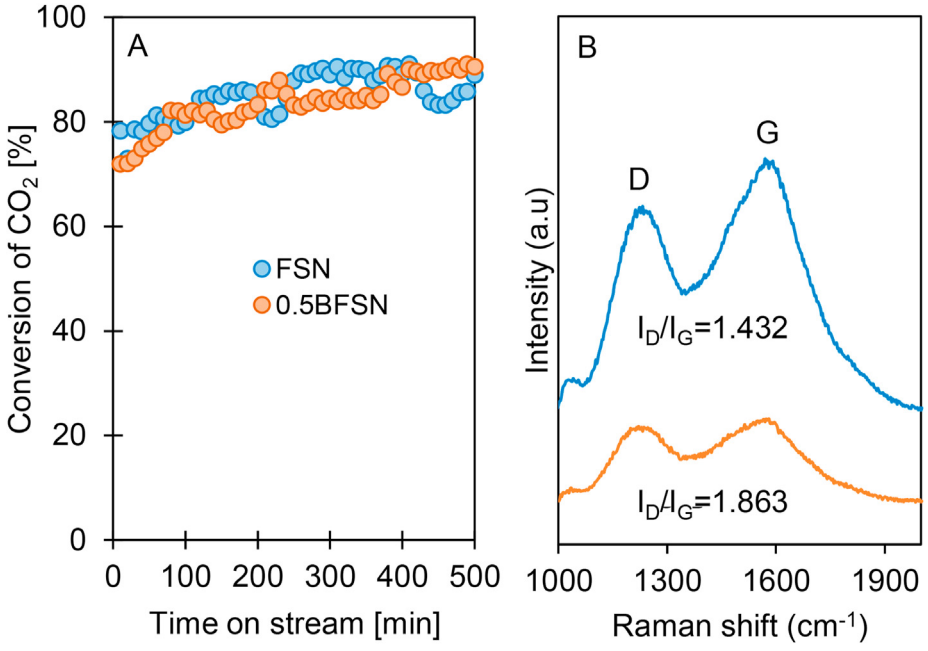

Fig. 8 – (A) Stability test of FSN based catalyst. The catalytic testing was. conducted at GHSV = 13,500 mL g-1 h-1, CO2:H2 = 1:4. (B) Raman spectra for both catalysts.

Table 2 – Comparison of activity of different catalysts for CO_2 hydrogenation to methane.

Catalysts	Temperature (°C)	Pressure (MPa)	H_2: CO_2	GHSV (mL g^{-1} h^{-1})	Y_{CH4} (%)	Ref
0.5B-FSN	525	0.1	4	13,500	85	This work
Ni/SiO_2/GO	470	0.1	4	24,000	80	[6]
NiO/SBA-15	450	0.1	4	10,000	74	[9]
Ni/FSBA-15	450	0.1	4	24,900	98	[11]
Ru/HNS	450	0.1	4	12,000	60	[38]
Ni/SiO_2	500	0.1	4	60,000	68	[39]
Ni/SiO_2	500	0.1	4	40,000	70	[40]
Ni/La-Pr-Ce	400	0.1	4	100,000	60	[41]

compared to 0.5B-FSN (Fig. 6B) at all temperature range studied, confirming the higher adsorptivity of acidic CO_2 as well as the atomic hydrogen on the boron species at the surface of the latter catalyst. In addition, the intensities for those bands seem increased and decreased consecutively at elevated temperature, which in parallel with the intermittent appearance of small bands at around 3093 cm^{-1}, suggesting the simultaneous adsorption of CO_2 and rapid dissociation of molecule H_2 to atomic hydrogen to produce methane [36]. These results verified the significant role of boron on the FSN in accelerating and enhancing the CO_2 methanation. Schematically, the role of boron in the CO_2 methanation is proposed as in Fig. 7. The well-dispersed boron on the surface of nickel-fibrous silica catalyst, as shown by the boron mapping image in Fig. 3E and J enhanced the CO_2 adsorption, which then accelerated the formation of such bridged or/and chelated bidentate carbonates, hydrogen carbonate as well as formates when reacted with the hydrogen atom that split on the nickel surface [35,37]. This phenomenon was evidenced by the shouldered bands fluctuations at 1680-1600 cm^{-1} shown in Fig. 6. The dehydration of these intermediates then formed C–H bonded species which subsequent serial hydrogenation gave the final product of methane.

Stability studies

The stability test of both catalysts is presented in Fig. 8A, the CO_2 conversion is plotted as a function of the time on stream. The reaction was carried out at 350 °C for more than 100 h in order to keep the CO_2 conversion below 100%. Obviously, the stability of 0.5B-FSN is comparable with the pristine FSN. However, further inspection of the spent catalysts on Raman spectroscopy (Fig. 8B) demonstrated that the spectrum for 0.5B-FSN is lower, indicating its more coke-resistance than the pristine FSN. The G band of pure FSN is more intense than the D band, indicating that carbon nanotubes and amorphous carbon may have developed on the catalytic surface. In addition, the higher I_D/I_G ratio of 0.5B-FSN also illustrates the defective nature of 0.5B-FSN due to its porous structure. These results evidently could explain the higher performance of 0.5B-FSN compared to FSN shown in Fig. 1.

Furthermore, to highlight the catalyst's superiority in this work, the optimal 0.5B-FSN was compared with the reported catalysts (Table 2). The CO_2 hydrogenation to methane over all the catalysts was conducted at 0.1 MPa and using $H_2/CO_2 = 4$. The methane yield of 0.5B-FSN was competitive with the literature data [6,11], and the space velocity used is lowered amongst the catalyst mentioned. However, Liu and Tian [9] reported that NiO/SBA-15 catalyst possess relatively poor catalytic activity even at a low space velocity of 10,000 mL g^{-1} h^{-1}. Similarly, Ru/HNS catalyst showed a lower yield of CH_4 (60%) at lower space velocity (12,000 mL g^{-1} h^{-1}) [38]. In contrast, even though the higher space velocity was applied, the CH_4 yield was still low [39–41]. From the above comparison, 0.5B-FSN catalyst is deemed as the prospective catalyst demonstrating remarkable CO_2 methanation activity in terms of CH_4 yield, accredited to its appropriate dispersion of boron surrounds the nickel particles, which improve the adsorption of CO_2.

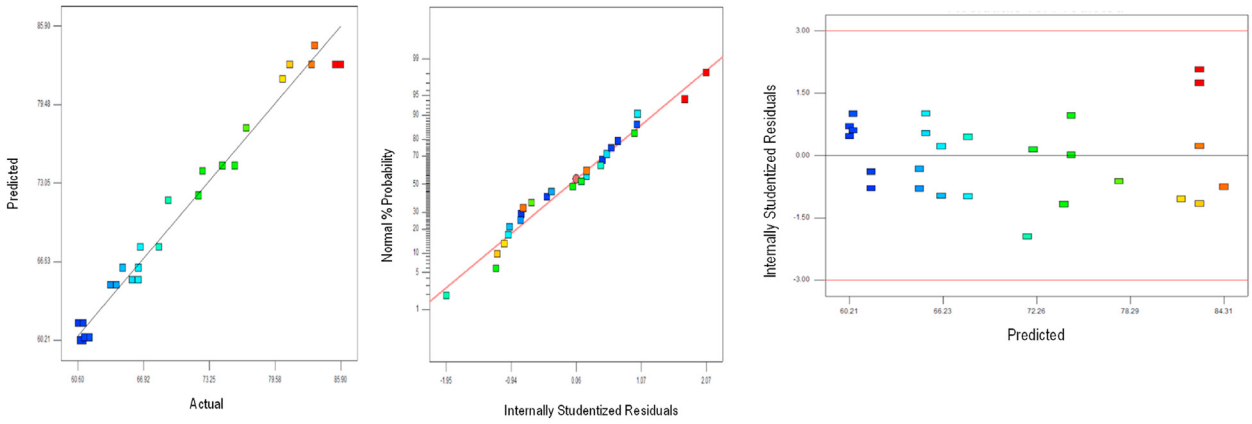

Fig. 9 – (A) Scatter diagram of predicted response versus actual, (B) Normal % probability plot, and (C) Internally studentized residuals for the yield of CH_4.

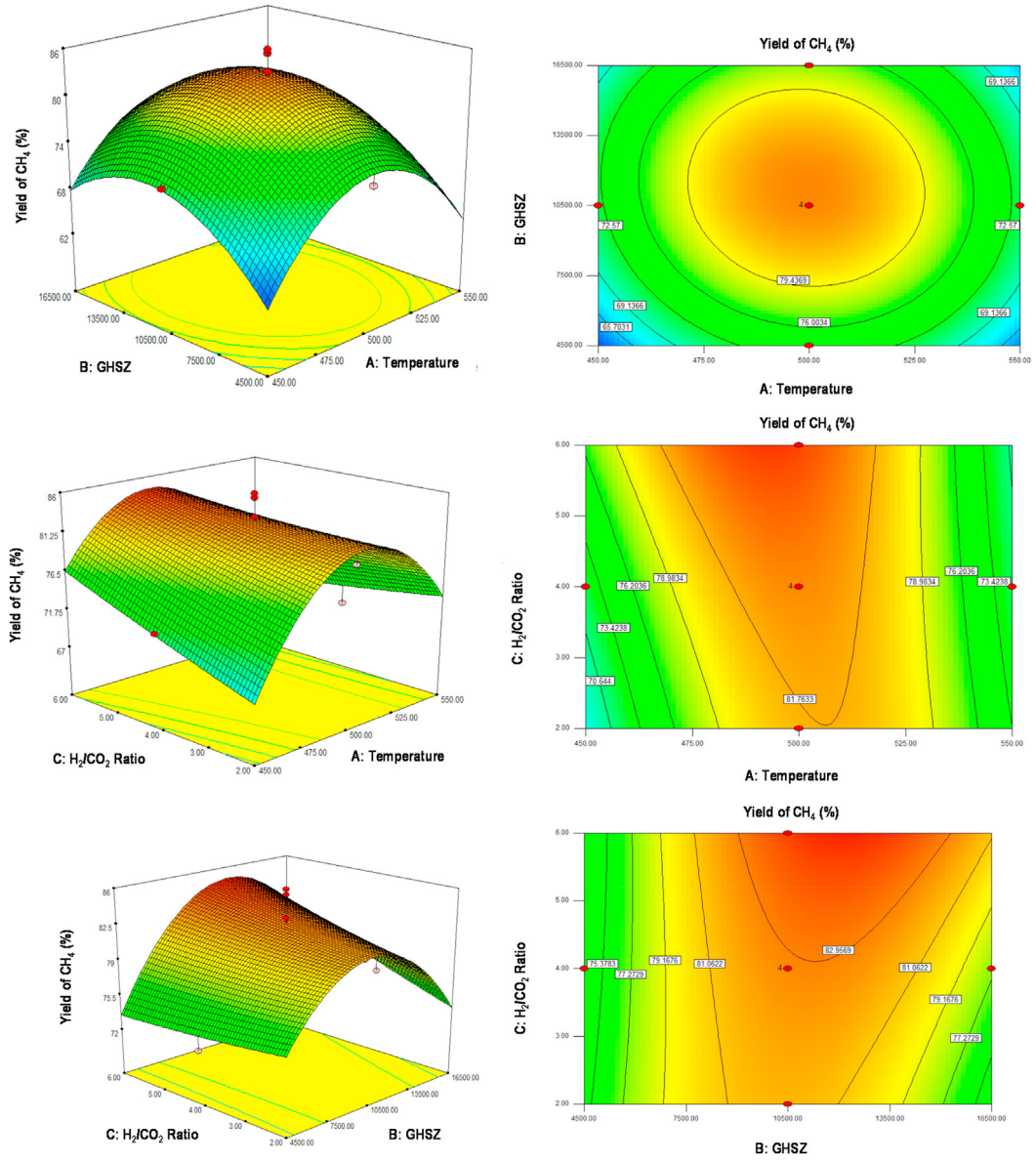

Fig. 10 – Response surface plots for CO_2 methanation over 0.5B-FSN showing interaction between (A) H_2/CO_2 ratio and temperature (B) H_2/CO_2 ratio and GHSV (C) GHSV and temperature.

Statistical analysis

During a set of trials, the traditional way of optimizing multifactor experiments includes altering a single factor while keeping all other factors constant. Because the various interactions between the variables are not taken into account, this method is time expensive and impractical for determining the genuine optimum value. As a result, an FCCCD was used in conjunction with an RSM to construct experiments on a statistical basis in this work. A small number of trials can be used to obtain the correlation between variables and responses, which can then be easily displayed using the surface contour plot. Herein, the optimization was carried out via FCCCD under 26 runs of experiments over 0.5B-FSN catalyst with three independent parameters: reaction temperature (A), GSHV (B), and H_2/CO_2 ratio (C). The experimental results at corresponding experimental conditions were indicated in Table S2, along with the design response (Yield CH_4, Y).

The final regression function for response in terms of coded factors and actual factors was constructed as Eq. (4) and Eq. (5), respectively, using regression analysis to fit the response.

$$Yield\ CH_4 = 82.76 - 0.18A + 1.77B - 1.37C - 1.02AB - 2.97AC + 2.10BC - 10.91A^2 - 6.96B^2 + 0.19C^2 \quad (4)$$

$$\begin{aligned} \textit{Yield } CH_4 = & -1103.38410 + 4.51706\,(Temperature) \\ & + 5.36548^{3}(GHSV) + 13.35288\left(\frac{CO_2}{H_2}\right) \\ & - 3.41667^{6}(Temperature * GHSV) \\ & - 0.029750\left(Temperature * \frac{CO_2}{H_2}\right) \\ & + 1.75000^{4}\left(GHSV * \frac{CO_2}{H_2}\right) \\ & - 4.36585^{3}(Temperature^2) \\ & - 1.93462^{7}(GHSV^2) + 0.046341\left(\frac{{CO_2}^2}{H_2}\right) \end{aligned} \quad (5)$$

Upon implying this process, the results were obtained in the form of analysis of variance (ANOVA), suggesting the effect of parameters and their interaction. ANOVA was used to assess the statistical significance of the FCCCD model, as shown in Table S3, which also included a quadratic response surface model that can be utilized to navigate the design space. The larger calculated F−value (F_{model} = 72.18) as opposed to the tabulated F−value (F_{table} = 2.55) for the considered probability (p = 0.05) and degree of freedom suggests that the quadratic regression model was significant, as demonstrated by ANOVA results. Based on the significant p−values, it can be concluded that the quadratic polynomial models, particularly A^2 and B^2 provided a good approximation for the investigated response, as they are in excellent agreement with reasonably high coefficients of multiple determination (R^2) of 0.98%, close to 1 for the yield of CH_4. The predicted R^2 (0.94) was found to be an inequitable agreement with the adjusted R^2 (0.96), implying that this model was a good statistical one [42].

Because the majority of the points were positioned on the plot's straight line, the results from the predicted against actual plot depicted in Fig. 9A showed an excellent correlation between actual and predicted values. As a result, the models are deemed adequate for predicting and optimizing methanation [43]. Fig. 9B also depicted the plot of the normal probability of the CH_4 yield in order to assess the competency fit for the proposed model. The normal distribution of residuals with acceptable equal variance is revealed by the trend depicted in this figure. Apart from equal scatter above and below the x-axis, Fig. 9C shows no obvious pattern or unusual structure. This indicates that the proposed model is sufficient, and there is no reason to believe that the independence or constant variance assumptions have been violated [42].

The effect of several process factors on the production of CH_4 may be seen in the contour and three-dimensional surface plots (Fig. 10). The increase in temperature (A) and GHSV (B) seem increased the yield of CH_4 with the maximum yield of 84.31% was achieved at 500 °C and GHSV of 10,500 mL g^{-1} h^{-1}, respectively. Due to CO_2 methanation is exothermic in nature, further increased of both variables reduced the yield of CH_4. While, keep increasing the H_2/CO_2 ratio to a maximum 6:1 and temperature until 500 °C increased the yield of CH_4 to a maximum 81.76%. However, the yield of CH_4 decreased by a further increase in temperature, this may be due to the reaction reversed to produce syngas. Similar results were observed when the H_2/CO_2 ratio was interacted with GHSZ, whereby the maximum yield of CH_4 was achieved at GHSV of 10,500 mL g^{-1} h^{-1}.

Based on the abovementioned results, the optimum condition was obtained at temperature 500 °C, GHSV of 10,500 mL g^{-1} h^{-1}, and H_2/CO_2 ratio of 6, attaining the highest percentage of CH_4 at 84.31% (Table S4). Four confirmation runs were carried out to ensure that the model was adequate (Table S5). To determine the error, the predicted values were compared to the experimental values, yielding a literally minimal error ranging from 0.46 to 11.43%. As a result, the created empirical models for CO_2 hydrogenation to CH_4 were reasonably accurate, as all actual values for the confirmation runs were within the 94% prediction interval.

Conclusion

In this study, boron was loaded onto a fibrous-silica-nickel (B-FSN) catalyst, and its behaviour on the FSN surface was examined in detail towards CO_2 hydrogenation to methane. Characterization results exhibited that the appropriate boron dispersion near the nickel particles is an important factor in enhancing the methanation. From the in-situ FTIR study, it could be decided that the adsorption of CO_2 was accelerated onto boron which afterward cooperated with the dissociated hydrogen atom from the nickel species to form intermediates before dehydrating and performing consecutive hydrogenation to give the final product of methane. These sequential reactions occurred rapidly, thus the coke formation could be controlled. The optimization via the hybrid approach of the FCCCD and RSM presented that reaction using H_2/CO_2 ratio of 6, GHSV of 10,500 mL g^{-1} h^{-1}, at 500 °C gave the highest percentage of CH_4 of 84.3%. The less error between predicted and experimental values (<11%) revealed that the developed empirical models were reasonably accurate for CO_2 methanation.

Declaration of competing interest

The authors declare that they have no known competing financial interests or personal relationships that could have appeared to influence the work reported in this paper.

Acknowledgement

The authors are appreciative for the High Impact Research Grant (Grant No. 08G92) and Professional Development Research University Grant (No. 05E44) from Universiti Teknologi Malaysia.

Appendix A. Supplementary data

Supplementary data to this article can be found online at https://doi.org/10.1016/j.ijhydene.2022.02.126.

REFERENCES

[1] Ye RP, Liao L, Reina TR, Liu J, Chevella D, Jin Y, Liu J. Engineering Ni/SiO_2 catalysts for enhanced CO_2 methanation. Fuel 2021;285:119151. https://doi.org/10.1016/j.fuel.2020.119151.

[2] Bacariza MC, Graça I, Bebiano SS, Lopes JM, Henriques C. Micro- and mesoporous supports for CO_2 methanation catalysts: a comparison between SBA-15, MCM-41 and USY zeolite. Chem Eng Sci 2018;175:72–83. https://doi.org/10.1016/j.ces.2017.09.027.

[3] Fukuhara C, Kamiyama A, Itoh M, Hirata N, Ratchahat S, Sudoh M, Watanabe R. Auto-methanation for transition-metal catalysts loaded on various oxide supports: a novel route for CO_2 transformation at room-temperature and atmospheric pressure. Chem Eng Sci 2020;219:115589. https://doi.org/10.1016/j.ces.2020.115589.

[4] Lim JY, McGregor J, Sederman AJ, Dennis JS. Kinetic studies of the methanation of CO over a Ni/γ-Al_2O_3 catalyst using a batch reactor. Chem Eng Sci 2016;146:316–36. https://doi.org/10.1016/j.ces.2016.02.001.

[5] Nagai M, Nakahira K, Ozawa Y, Namiki Y, Suzuki Y. CO_2 reforming of methane on Rh/Al_2O_3 catalyst. Chem Eng Sci 2007;62:4998–5000. https://doi.org/10.1016/j.ces.2006.12.017.

[6] Ma H, Ma K, Ji J, Tang S, Liu C, Jiang W, Yue H, Liang B. Graphene intercalated Ni-SiO_2/GO-Ni-foam catalyst with enhanced reactivity and heat-transfer for CO_2 methanation. Chem Eng Sci 2019;194:10–21. https://doi.org/10.1016/j.ces.2018.05.019.

[7] Aziz MAA, Jalil AA, Triwahyono S, Saad MWA. CO_2 methanation over Ni-promoted mesostructured silica nanoparticles: influence of Ni loading and water vapor on activity and response surface methodology studies. Chem Eng J 2015;260:757–64. https://doi.org/10.1016/j.cej.2014.09.031.

[8] Hamid MYS, Jalil AA, Rahman AFA, Abdullah TAT. Enhanced reactive CO_2 species formation via V_2O_5-promoted Ni/KCC-1 for low temperature activation of CO_2 methanation. React Chem Eng 2019;4:1126–35. https://doi.org/10.1039/C8RE00312B.

[9] Liu Q, Tian Y. One-pot synthesis of NiO/SBA-15 monolith catalyst with a three-dimensional framework for CO_2 methanation. Int J Hydrogen Energy 2017;42:12295–300. https://doi.org/10.1016/j.ijhydene.2017.02.070.

[10] Shafiee P, Alavi SM, Rezaei M. Solid-state synthesis method for the preparation of cobalt doped Ni–Al_2O_3 mesoporous catalysts for CO_2 methanation. Int J Hydrogen Energy 2021;46(5):3933–44. https://doi.org/10.1016/j.ijhydene.2020.10.221.

[11] Bukhari SN, Chong CC, Setiabudi HD, Cheng YW, The LP, Jalil AA. Ni/Fibrous type SBA-15: highly active and coke resistant catalyst for CO_2 methanation. Chem Eng Sci 2021;229:116141. https://doi.org/10.1016/j.ces.2020.116141.

[12] Sidik SM, Triwahyono S, Jalil AA, Aziz MAA, Fatah NAA, The LP. Tailoring the properties of electrolyzed Ni/mesostructured silica nanoparticles (MSN) via different Ni-loading methods for CO_2 reforming of CH_4. J CO_2 Util 2016;13:71–80. https://doi.org/10.1016/j.jcou.2015.12.004.

[13] Hassan NS, Jalil AA, Aziz FFA, Aziz MAH, Hussain I, Ali MW. New insight into sequential of silica-zirconia precursors in stabilizing silica-doped tetragonal zirconia nanoparticles for enhanced photoactivity. Mater Lett 2021;291:129582. https://doi.org/10.1016/j.matlet.2021.129582.

[14] Siang TJ, Bach LG, Singh S, Truong QD, Phuc NHH, Alenazey F, Vo DVN. Methane bi-reforming over boron-doped Ni/SBA-15 catalyst: longevity evaluation. Int J Hydrogen Energy 2019;44:20839–50. https://doi.org/10.1016/j.ijhydene.2018.06.123.

[15] Wu J, Qin L, Wang C, Lv B, Wang L, Chen J, Xu Y. Ultrathin N-rich boron nitride nanosheets supported iron catalyst for Fischer–Tropsch synthesis. RSC Adv 2016;6:38356–64. https://doi.org/10.1039/C6RA05517F.

[16] Chien AC, van Bokhoven JA. Boron nitride coated rhodium black for stable production of syngas. Catal Sci Technol 2015;5:3518–24. https://doi.org/10.1039/C5CY00021A.

[17] Aly M, Fornero EL, Leon-Garzon AR, Galvita VV, Saeys M. Effect of boron promotion on coke formation during propane dehydrogenation over Pt/γ-Al_2O_3 catalysts. ACS Catal 2020;10:5208–16. https://doi.org/10.1021/acscatal.9b05548.

[18] Huo Y, Zhang Y, Wang C, Fang Y, Li K, Chen Y. Boron-doping effect on the enhanced hydrogen storage of titanium-decorated porous graphene: a first-principles study. Int J Hydrogen Energy 2021;46(80):40301–11. https://doi.org/10.1016/j.ijhydene.2021.09.243.

[19] Fouskas A, Kollia M, Kambolis A, Papadopoulou C, Matralis H. Boron-modified Ni/Al_2O_3 catalysts for reduced carbon deposition during dry reforming of methane. Appl Catal Gen 2014;474:125–34. https://doi.org/10.1016/j.apcata.2013.08.016.

[20] Singh S, Nguyen TD, Siang TJ, Phuong PT, Phuc NHH, Truong QD, Vo DVN. Boron-doped Ni/SBA-15 catalysts with enhanced coke resistance and catalytic performance for dry reforming of methane. J Energy Inst 2020;93:31–42. https://doi.org/10.1016/j.joei.2019.04.011.

[21] Abdulrasheed AA, Jalil AA, Hamid MYS, Siang TJ, Fatah NAA, Izan SM, Hassan NS. Dry reforming of methane to hydrogen-rich syngas over robust fibrous KCC-1 stabilized nickel catalyst with high activity and coke resistance. Int J Hydrogen Energy 2020;45:18549–61. https://doi.org/10.1016/j.ijhydene.2019.04.126.

[22] Fatah NAA, Triwahyono S, Jalil AA, Salamun N, Mamat CR, Majid ZA. n-Heptane isomerization over molybdenum supported on bicontinuous concentric lamellar silica KCC-1: influence of phosphorus and optimization using response surface methodology (RSM). Chem Eng J 2017;314:650–9. https://doi.org/10.1016/j.cej.2016.12.028.

[23] Aziz MAA, Jalil AA, Triwahyono S, Mukti RR, Taufiq-Yap YH, Sazegar MR. Highly active Ni-promoted mesostructured silica nanoparticles for CO_2 methanation. Appl Catal B Environ 2014;147:359–68. https://doi.org/10.1016/j.apcatb.2013.09.015.

[24] El-Kemary M, Nagy N, El-Mehasseb I. Nickel oxide nanoparticles: synthesis and spectral studies of interactions with glucose. Mater Sci Semicond Process 2013;16:1747–52. https://doi.org/10.1016/j.mssp.2013.05.018.

[25] Liu B, Xie K, Oh SC, Sun D, Fang Y, Xi H. Direct synthesis of hierarchical USY zeolite for retardation of catalyst deactivation. Chem Eng Sci 2016;153:374–81. https://doi.org/10.1016/j.ces.2016.07.041.

[26] Sing KSW. Reporting physisorption data for gas/solid systems with special reference to the determination of surface area and porosity (Recommendations 1984). Pure Appl Chem 1985;57:603–19. https://doi.org/10.1351/pac198557040603.

[27] Fatah NAA, Jalil AA, Salleh NFM, Hamid MYS, Hassan ZH, Nawawi MGM. Elucidation of cobalt disturbance on Ni/Al_2O_3 in dissociating hydrogen towards improved CO_2 methanation and optimization by response surface

methodology (RSM). Int J Hydrogen Energy 2019. https://doi.org/10.1016/j.ijhydene.2019.04.119.
[28] Ghani NNM, Jalil AA, Triwahyono S, Aziz MAA, Rahman AFA, Hamid MYS, Izan SM, Nawawi MGM. Tailored mesoporosity and acidity of shape-selective fibrous silica beta zeolite for enhanced toluene co-reaction with methanol. Chem Eng Sci 2019;193:217–29. https://doi.org/10.1016/j.ces.2018.09.009.
[29] Kamarudin NHN, Jalil AA, Triwahyono S, Salleh NFM, Karim AH, Mukti RR, Hameed BH, Ahmad A. Role of 3-aminopropyltriethoxysilane in the preparation of mesoporous silica nanoparticles for ibuprofen delivery: effect on physicochemical properties. Microporous Mesoporous Mater 2013;180:235–41. https://doi.org/10.1016/j.micromeso.2013.06.041.
[30] Izan SM, Triwahyono S, Jalil AA, Majid ZA, Fatah NAA, Hamid MYS, Ibrahim M. Additional Lewis acid sites of protonated fibrous silica@ BEA zeolite (HSi@ BEA) improving the generation of protonic acid sites in the isomerization of C_6 alkane and cycloalkanes. Appl Catal Gen 2019;570:228–37. https://doi.org/10.1016/j.apcata.2018.11.028.
[31] Triwahyono S, Jalil AA, Izan SM, Jamari NS, Fatah NAA. Isomerization of linear C5–C7 over Pt loaded on protonated fibrous silica@ Y zeolite (Pt/HSi@ Y). J Energy Chem 2019;37:163–71. https://doi.org/10.1016/j.jechem.2019.02.016.
[32] Sayari A, Moudrakovski I, Danumah C, Ratcliffe CI, Ripmeester JA, Preston KF. Synthesis and nuclear magnetic resonance study of boron-modified MCM-41 mesoporous materials. J Phys Chem 1995;99:16373–9. https://doi.org/10.1021/j100044a026.
[33] Hussain I, Jalil AA, Hassan NS, Hambali HU, Jusoh NWC. Fabrication and characterization of highly active fibrous silica-mordenite (FS@SiO_2-MOR) cockscomb shaped catalyst for enhanced CO_2 methanation. Chem Eng Sci 2020;228:115978. https://doi.org/10.1016/j.ces.2020.115978.
[34] Prymak I, Kalevaru VN, Wohlrab S, Martin A. Continuous synthesis of diethyl carbonate from ethanol and CO $_2$ over Ce-Zr-O. Catal Sci Technol 2015;5:2322–31. https://doi.org/10.1039/C4CY01400F.
[35] Hamid MYS, Triwahyono S, Jalil AA, Jusoh NWC, Izan SM, Abdullah TAT. Tailoring the properties of metal oxide loaded/KCC-1 toward a different mechanism of CO_2 methanation by in situ IR and ESR. Inorg Chem 2018;57:5859–69. https://doi.org/10.1021/acs.inorgchem.8b00241.
[36] Fatah NAA, Jalil AA, Triwahyono S, Yusof N, Mamat CR, Izan SM, Nabgan W. Favored hydrogenation of linear carbon monoxide over cobalt loaded on fibrous silica KCC-1. Int J Hydrogen Energy 2020;45:9522–34. https://doi.org/10.1016/j.ijhydene.2020.01.144.
[37] Aziz MAA, Jalil AA, Triwahyono S, Ahmad A. CO_2 methanation over heterogeneous catalysts: recent progress and future prospects. Green Chem 2015;17:2647–63. https://doi.org/10.1039/c5gc00119f.
[38] Tang Y, Men Y, Liu S, Wang J, Wang K, Li Y, An W. Morphology-dependent support effect of Ru/MnO_x catalysts on CO_2 methanation. Colloids Surf A Physicochem Eng 2021;630:127636. https://doi.org/10.1016/j.colsurfa.2021.127636.
[39] Zhang Y, Liu Q. Nickel phyllosilicate derived Ni/SiO_2 catalysts for CO_2 methanation: identifying effect of silanol group concentration. J CO_2 Util 2021;50:101587. https://doi.org/10.1016/j.jcou.2021.101587.
[40] Wang K, Men Y, Liu S, Wang J, Li Y, Tang Y, Li L. Decoupling the size and support/metal loadings effect of Ni/SiO_2 catalysts for CO_2 methanation. Fuel 2021;304:121388. https://doi.org/10.1016/j.fuel.2021.121388.
[41] Siakavelas GI, Charisiou ND, AlKhoori A, AlKhoori S, Sebastian V, Hinder SJ, Goula MA. Highly selective and stable Ni/La-M (M= Sm, Pr, and Mg)-CeO_2 catalysts for CO_2 methanation. J CO_2 Util 2021;51:101618. https://doi.org/10.1016/j.jcou.2021.101618.
[42] Sukor NF, Jusoh R, Kamarudin NS. Intensification of phenolic acids extraction from Aleppo oak via probe type sonication method: kinetic, antioxidant and cost evaluation. Chem Eng Res Des 2021;166:227–36. https://doi.org/10.1016/j.cherd.2020.11.019.
[43] Demirel M, Kayan B. Application of response surface methodology and central composite design for the optimization of textile dye degradation by wet air oxidation. Int J Ind Chem 2012;3:1–10. https://doi.org/10.1186/2228-5547-3-24.